Intercluster Reactions between $Au_{25}(SR)_{18}$ and $Ag_{44}(SR)_{30}$

K. R. Krishnadas, Atanu Ghosh, Ananya Baksi, Indranath Chakraborty,[†] Ganapati Natarajan, and Thalappil Pradeep*

DST Unit of Nanoscience (DST UNS) and Thematic Unit of Excellence, Department of Chemistry, Indian Institute of Technology Madras, Chennai, 600 036, India

S *Supporting Information*

ABSTRACT: We present the first example of intercluster reactions between atomically precise, monolayer protected noble metal clusters using $Au_{25}(SR)_{18}$ and $Ag_{44}(SR)_{30}$ (RS− = alkyl/aryl thiolate) as model compounds. These clusters undergo spontaneous reaction in solution at ambient conditions. Mass spectrometric measurements both by electrospray ionization and matrix assisted laser desorption ionization show that the reaction occurs through the exchange of metal atoms and protecting ligands of the clusters. Intercluster

alloying is demonstrated to be a much more facile method for heteroatom doping into $Au_{25}(SR)_{18}$, as observed by doping up to 20 Ag atoms. We investigated the thermodynamic feasibility of the reaction using DFT calculations and a tentative mechanism has been presented. Metal core-thiolate interfaces in these clusters play a crucial role in inducing these reactions and also affect rates of these reactions. We hope that our work will help accelerate activities in this area to establish chemistry of monolayer protected clusters.
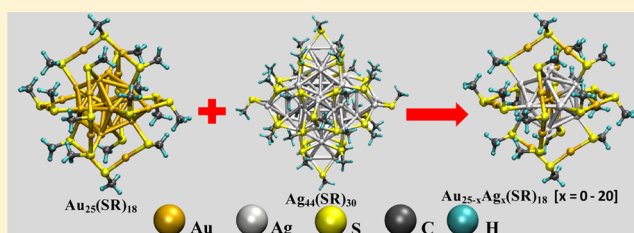
INTRODUCTION

Intercluster reactions between metal clusters are rare, and their chemistry is mostly explored through reactions with small molecules.[1] Monolayer protection[2] with suitable ligands facilitated the synthesis of highly stable, atomically precise metal clusters in sufficient quantities. This opened up a way to develop an in-depth understanding of their chemistry, conveniently in the solution phase. Reactions of these clusters in solutions are expected to complement the results obtained from gas phase experiments, providing further insights into their properties. Moreover, cluster chemistry in solution has practical applications.[3,4] Among the ligand-protected metal clusters, thiolate-protected noble metal clusters ($Au_{25}(SR)_{18}$, for example) have been recognized as a distinct category in view of their unique properties.[5] The earliest of the chemistry of these clusters has been ligand exchange,[6] leading to an understanding of the localization of electronic transitions to the Au_nS_m moiety and demonstration of fluorescence resonance energy transfer (FRET).[6i] Though there have been a few attempts dealing with the reactions of these clusters with halocarbons,[7] metal ions,[8,9] metal−thiolates,[10a] salts[10b] and one-dimensional nanostructures,[11] there has been no example of intercluster chemistry.

EXPERIMENTAL SECTION

Materials. Chloroauric acid trihydrate ($HAuCl_4.3H_2O$) was purchased from Sigma-Aldrich. Silver nitrate ($AgNO_3$) was purchased from RANKEM India. 2-phenylethanethiol (PET), n-butanethiol (n-BuSH), 4-fluorothiophenol (FTP), 4-mercaptobenzoic acid (MBA), tetraoctylammonium bromide (TOAB), tetraphenylphosphonium bromide (PPh_4Br), sodium borohydride ($NaBH_4$) were purchased

from Sigma-Aldrich. All the solvents used (tetrahydrofuran (THF), methanol, hexane, dichloromethane (DCM) and dimethylformamide (DMF)) were of analytical grade.

Synthesis of Clusters. $Au_{25}(PET)_{18}$ and $Au_{25}(BuS)_{18}$: 2 mL of 50 mM $HAuCl_4.3H_2O$ in THF was diluted to 7.5 mL using THF. About 65 mg of TOAB was added to this solution and stirred at 1500 rpm for 30 min at room temperature. The initial yellow color of the solution turned deep red during stirring. About 0.5 mmol of pure thiol was added at a stretch while stirring at the same speed. The deep red color slowly turned to yellow and eventually became colorless after about 45 min. After stirring further for 2 h, 2.5 mL of ice cold aqueous $NaBH_4$ (0.2 M) was added in one lot. The solution turned black immediately and stirring was continued for 5 h. The solution was rotary evaporated and precipitated with methanol, washed repeatedly with the same and dried.

$Au_{25}(FTP)_{18}$. Five mg of $Au_{25}(n$-BuS$)_{18}$ was dissolved in 0.5 mL of toluene and 150 times (by weight) of pure 4-fluorothiophenol was added to it. The solution was heated at 50 °C in an oil bath while stirring. After about 25 min, clusters were precipitated with hexane and collected by centrifugation. This precipitate was washed with hexane, dissolved in DCM and centrifuged to remove thiolates. This cluster solution was vacuum-dried and stored at 4 °C.

$[PPh_4]_4[Ag_{44}(FTP)_{30}]$. The cluster was synthesized following a solid state route.[21] 20 mg of $AgNO_3$ and 12 mg of PPh_4Br were ground thoroughly in an agate mortar and pestle for 5 min. About 76 μL of 4-fluorothiophenol was added to it in one shot and the mixture was ground for about 3 more minutes. Dry $NaBH_4$ (45 mg) was added and the mixture was ground until the pasty mass became brown in color. This was extracted with 7 mL of dichloromethane and kept undisturbed at room temperature until UV/vis spectra showed all the characteristic features of the cluster. The clusters were purified
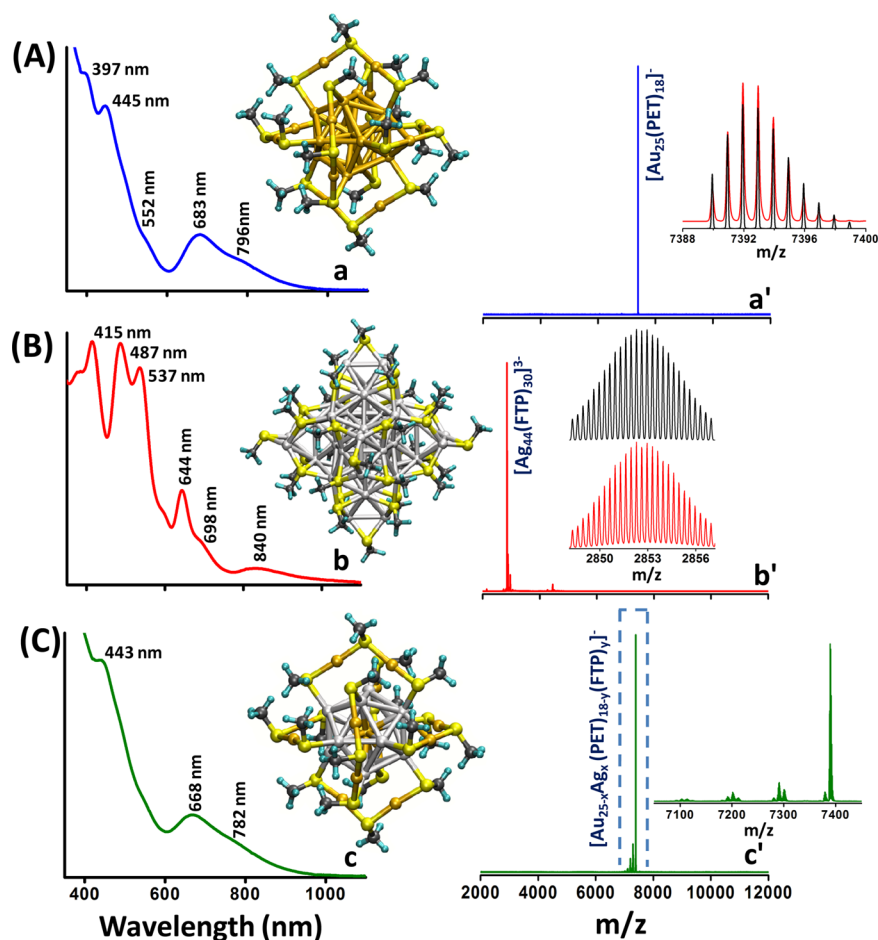
Figure 1. UV/vis absorption and negative ion ESI MS spectra of $Au_{25}(PET)_{18}$ (A), $Ag_{44}(FTP)_{30}$ (B) and their 14:1 molar mixture (C) showing changes in the spectral features due to intercluster reaction. In A−C, panels a−c and a′−c′ are the UV/vis and ESI MS spectra, respectively. Characteristic peak positions are marked. The corresponding clusters are also shown in between the spectra (modeled assuming the coordinates from the crystal structures). Color codes for the atoms in the inset pictures: Light yellow = sulfur, orange = gold, gray = silver, black = carbon, and cyan = hydrogen. For simplicity, we assumed -SMe ligands, instead of PET and FTP ligands. Inset of a′ shows the molecular ion region (m/z 7388−7400) of $Au_{25}(PET)_{18}$, showing isotope resolution. Inset of b′ shows the same for $Ag_{44}(FTP)_{30}$ in the 3^- charge region (m/z 2848−2857). Theoretical (black) and experimental (red) spectra of ions are compared. The spectra corresponding to the product (marked in open rectangles) is expanded in the inset of c′.

adopting the same protocol used for $Au_{25}(SR)_{18}$. $Na_4[Ag_{44}(MBA)_{30}]$ was synthesized following a reported method[2e] with slight modifications, as described in Supporting Information.

Intercluster Reactions. Stock solutions of clusters were prepared in dichloromethane, except for $Ag_{44}(MBA)_{30}$ which was prepared in DMF. Required volumes of each of the stock solutions were added into 1 mL of dichloromethane at room temperature and the mixture was stirred with a pipette. It was not stirred magnetically. The reaction occurred immediately after mixing as observed from the immediate color changes and time-dependent MALDI MS and ESI MS measurements. All reactions were carried out at room temperature (~30 °C).

Mass Spectral Measurements. We performed matrix assisted laser desorption ionization (MALDI) and electrospray ionization (ESI) mass spectrometry (MS) measurements. We used Applied Biosystems Voyager DEPro (MALDI) and Waters Synapt G2-Si (ESI and MALDI) mass spectrometers. ESI MS had a maximum resolution of 50 000 in the mass range of interest. More details about the measurements are given in Supporting Information.

Computational Details. We used density functional theory (DFT) as implemented in the real-space grid-based projector augmented wave (GPAW) package.[28] Full computational details can be found in the Supporting Information. We calculated the energy difference between the unexchanged cluster and a single Ag atom

exchanged $[Au_{25}(SR)_{18}]^-$ and a single Au atom exchanged $[Ag_{44}(SR)_{30}]^{4-}$, for each of the isomers. The three symmetry-unique positions for the Ag atom in $[Au_{25}(SR)_{18}]^{1-}$ were the central atom (denoted by C), icosahedral vertex atom (I), and the staple gold atom (S). The four symmetry unique positions in $[Ag_{44}(SR)_{30}]^{4-}$ for the Au atom were the outermost shell in the middle dodecahedron (S), one of the eight cubic vertex positions (D_{cv}) and one of the 12 cube-face capping atoms (D_{cf}), and last, atoms in inner icosahedron (I) (see Figure S28). We calculated the energy of the overall reaction for the case of a single metal atom exchange in each combination of final substituent positions. We also calculated the energies of the substitution reactions of a single metal atom and single metal–ligand fragment, Ag and Ag-SR into $[Au_{25}(SR)_{18}]$, or, Au and Au-SR into $[Ag_{44}(SR)_{30}]^{4-}$ for each of the symmetry-unique positions mentioned above. To investigate the feasibility of electron transfer in this system, we compared the relative energies of the HOMO and LUMO states, for both $[Au_{25}(SR)_{18}]^-$and $[Ag_{44}(SR)_{30}]^{4-}$, and their alloys.

■ RESULTS AND DISCUSSION

(A). Reactions between Clusters Having Different Ligands. Initially we studied the reaction between $Au_{25}(PET)_{18}$ and $Ag_{44}(FTP)_{30}$ prepared as described in the Experimental Section. PET and FTP are the ligands protecting

Au$_{25}$ and Ag$_{44}$ clusters, respectively (see the Experimental Section). Appropriate volumes of their stock solutions were added into a fixed volume of dichloromethane at room temperature (~30 °C) (see Experimental Section for details) to get defined concentrations of the reacting species. UV/visible (UV/vis) absorption features and electrospray ionization mass spectra (ESI MS) of the clusters before and immediately after (within 1 min) mixing are shown in Figure 1. The molecular ion peak of Au$_{25}$(PET)$_{18}$ at m/z 7391 is shown in trace a′ of Figure 1A along with the expanded isotopically resolved molecular ion. Typical fragmentation pattern of Au$_{25}$(PET)$_{18}$ shown in Supporting Information (Figure S1) proves the identity of the cluster. Optical absorption spectrum of Au$_{25}$(PET)$_{18}$ shows characteristic peaks[2c] at 796, 683, 552, 445, and 397 nm (trace a in Figure 1A). Similarly, Ag$_{44}$(FTP)$_{30}$ is characteristic in its optical absorption spectrum[2e−g] (trace b, Figure 1B). [Ag$_{44}$(FTP)$_{30}$]$^{3−}$ was the prominent feature in the ESI MS of Ag$_{44}$(SR)$_{30}$ (trace b′, Figure 1B). Isotope distributions of the prominent features of these clusters match well with the theoretical patterns as shown in the insets. For example, the spectrum in the m/z 7388−7400 window of Au$_{25}$(PET)$_{18}$ (inset of trace a′ in Figure 1A) shows all the isotope features of the molecular ion. Detailed assignment of the spectrum in trace b′ of Figure 1B is given in Figure S2. Absorption features of Au$_{25}$(PET)$_{18}$ changed significantly and those due to Ag$_{44}$(FTP)$_{30}$ were not observed at all upon mixing the two clusters (trace c in Figure 1C). Comparing the ESI MS spectra in Figure 1A−C, we notice that a series of peaks at m/z lower than Au$_{25}$(PET)$_{18}$ appeared immediately after mixing. (description of these peaks follows later). These changes in the absorption and mass spectral features confirm that the clusters react with each other spontaneously in solution. Time-dependent changes during the reaction at various Au$_{25}$(PET)$_{18}$:Ag$_{44}$(FTP)$_{30}$ ratios (Figures S3−S5) show that a series of peaks at lower m/z than Au$_{25}$(PET)$_{18}$ (labeled as group I) and a broad feature at m/z higher than Ag$_{44}$(FTP)$_{30}$ (labeled as group II) appeared immediately after mixing the clusters. While a larger distribution of product peaks appeared in group I just after mixing, only 3−4 prominent peaks were observed after 10−15 min. The mass spectra after 1 h were similar to the spectra after 10−15 min, indicating that the reaction got equilibrated/completed in this time scale.

Reaction was studied at various Au$_{25}$(PET)$_{18}$:Ag$_{44}$(FTP)$_{30}$ ratios. MALDI MS spectra of Pthese reaction mixtures after 1 h of the reaction are shown in Figure 2. As the concentration of Ag$_{44}$(FTP)$_{30}$ was increased, the centroid of group I shifted continually toward lower m/z values. Simultaneously, intensity of group II increased. Peaks in group I of Figure 2 are expanded in the insets. Mass difference between these peaks is either 89 Da or 99 Da. The difference of 89 Da is due to the loss of an Au atom (197 Da) from Au$_{25}$(PET)$_{18}$ and a simultaneous inclusion of an Ag (108 Da) atom into it from Ag$_{44}$(FTP)$_{30}$. Mass difference of 99 Da is attributed to the loss of an Au-PET moiety (334 Da) and the inclusion of an Ag-FTP moiety (235 Da). Apart from these processes, there is a possibility for the exchange of ligands alone, i.e., FTP-PET exchanges. Because of the broadness of the MALDI MS peaks and small mass difference between FTP and PET ligands (10 Da), unambiguous confirmation of such exchange processes is not possible with MALDI MS measurements alone. Therefore, ESI MS measurements were carried out to reveal the details of the peaks in group I. Group II peaks will be discussed later in the text.
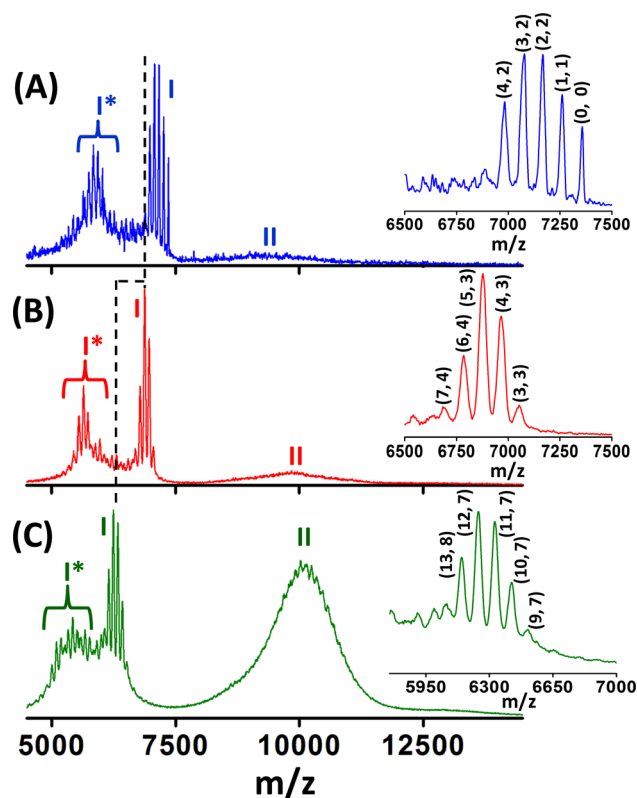
Figure 2. Negative ion mode MALDI MS spectra of the reaction mixtures for the Au$_{25}$(PET)$_{18}$:Ag$_{44}$(FTP)$_{30}$ ratio of (A) 14.0:1.0 (B) 7.0:1.0 and (C) 1.7:1.0. Each inset shows the expansion of the collection of peaks labeled I. The numbers (x, y) in parentheses (in the insets), correspond to the general molecular formula, Au$_{25−x}$Ag$_x$(PET)$_{18−y}$(FTP)$_y$. Shifts in the centroids of group I with increase in concentration of Ag$_{44}$(FTP)$_{30}$ are marked with dotted lines.

ESI MS of the reaction mixtures at various Au$_{25}$(PET)$_{18}$:Ag$_{44}$(FTP)$_{30}$ ratios are shown in Figure 3. Reaction products in the Au$_{25}$(PET)$_{18}$ region alone are shown here. Two features from each panel (marked in open rectangles) are expanded in the corresponding insets. Expanded features of the panels A−C are given in Figures S6−S9. These data reveal that each feature in these panels is a bunch of peaks separated by m/z 10. For example, the feature (2, 0−4) in Figure 3A is a collection of (2, 0), (2, 1), (2, 2), (2, 3) and (2, 4) peaks. The first number in parentheses of peak labels gives the number of Ag atoms exchanged. The second number gives the number of FTP ligands exchanged. MALDI MS measurements (Figure 2) indicated the presence of features separated by either m/z 89 or 99 and ESI MS measurements confirmed these features. For example, the peaks (1, 0), (2, 0), (3, 0), etc. and (1, 2), (2, 2), (3, 2), etc., are separated by m/z 89 Da (see Figure S10). Peaks such as (1, 1), (2, 2), (3, 3), etc. are separated by m/z 99. Mass difference of 89 Da is due to the Ag−Au exchange and the mass difference of 99 Da is due to (Au-PET)-(Ag-FTP) exchange, as mentioned earlier. Theoretical and experimental isotope patterns of peaks in the (2, 0−4) feature are shown in Figure S11 which further confirms the inclusion of the FTP ligand into Au$_{25}$(PET)$_{18}$. Thus, ESI MS measurements unambiguously confirm that the group I peaks observed in MALDI MS are due to the Ag−Au and (Ag-FTP)-(Au-PET) exchanges between Au$_{25}$(PET)$_{18}$ and Ag$_{44}$(FTP)$_{30}$. From Figure 3, we see that FTP-PET exchange is also occurring in Au$_{25}$(PET)$_{18}$ (see the feature (0, 0−3) in Figure 3A and
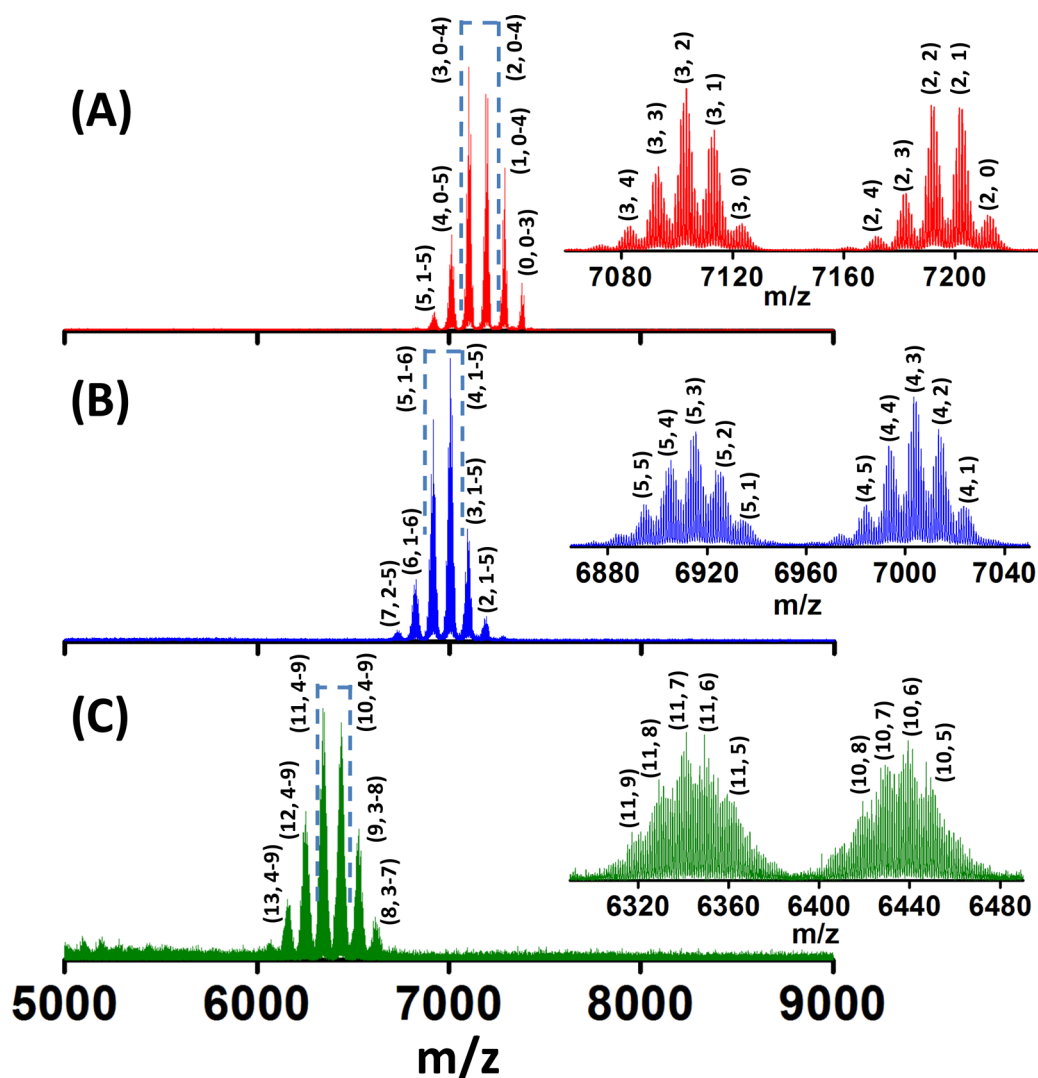
Figure 3. Negative ion mode ESI MS spectra of the reaction mixtures for the $Au_{25}(PET)_{18}$:$Ag_{44}(FTP)_{30}$ ratio of (A) 14.0:1.0 (B) 7.0:1.0 and (C) 1.7:1.0. Each inset shows the expansion of features marked in open rectangles. The numbers (x, y) in parentheses, are according to the general molecular formula, $Au_{25-x}Ag_x(PET)_{18-y}(FTP)_y$. Each peak (x, y) has its own isotope pattern and overlap of these features complicate the spectrum.

Figure S10), in addition to Ag−Au and (Ag-FTP)-(Au-PET) exchanges. This aspect will be discussed later. However, the total number of metal atoms and ligands were unchanged in the product clusters in group I. Hence, the series of peaks in group I have been assigned the general formula, $Au_{25-x}Ag_x(PET)_{18-y}(FTP)_y$. The larger the concentration of $Ag_{44}(FTP)_{30}$, the more Ag and FTP ligands are incorporated into $Au_{25}(PET)_{18}$. Inclusion of up to 1−5, 2−7 and 8−13 Ag atoms were observed for $Au_{25}(PET)_{18}$:$Ag_{44}(FTP)_{30}$ ratios of 14.0:1.0, 7.0:1.0 and 1.7:1.0, respectively. Insets of Figure 3 show that as the number of incorporated Ag atoms increases, peaks within a bunch become less resolved because of the isotope distribution of Ag. While distinct mass separations (of m/z 10) due to pure ligand exchange are seen in the reactions of clusters with differing ligands, these cannot be observed for clusters of the same ligands. We will revisit this aspect later in the text. Temporal changes in the absorption and luminescence spectra during reactions at various $Au_{25}(PET)_{18}$:$Ag_{44}(FTP)_{30}$ ratios are presented in Figures S12−S14. These results confirm the formation of $Au_{25-x}Ag_x(PET)_{18-y}(FTP)_y$ bimetallic clusters with mixed ligands.

The maximum numbers of Ag incorporations observed so far in the case of mixed ligand- and all thiolate-protected Au_{25} clusters[12−14] are 13 and 11, respectively. In contrast to these reports, we observed Ag doping of up to 13−16 and 16−20 atoms into $Au_{25}(SR)_{18}$ at higher concentrations of $Ag_{44}(FTP)_{30}$ (see Figures S15 and S16). Absorption spectra of these reaction mixtures are displayed in Figures S17 and S18, respectively. Thus, our experiments demonstrate for the first time that replacement of more than 13 Au atoms with Ag atoms is possible in Au_{25}. It is important to recall that the Au−Ag system is miscible in the entire composition window. This indicates that the intercluster reaction is much more facile in comparison to the coreduction methods used to synthesize $Au_{25-x}Ag_x(SR)_{18}$ clusters.

(B). Reaction between Clusters Having Same Ligands. While the products of intercluster reactions have been assigned in the earlier section, complications arise due to the simultaneous exchange of the metal atoms and the ligands. Definite confirmation of metal atom exchange is possible by using clusters containing the same ligands. For this purpose, we prepared $Au_{25}(FTP)_{18}$. Reactions of $Au_{25}(FTP)_{18}$ with $Ag_{44}(FTP)_{30}$ unambiguously confirm the incorporation of Ag

into $Au_{25}(FTP)_{18}$. MALDI MS and UV/vis spectra of $Au_{25}(FTP)_{18}$ shown in Figure S19 confirm the identity of the cluster. Time-dependent changes in the MALDI MS spectra of a mixture of these clusters are given in Figure S20. The mass spectra in the group I region after 1 and 3 h of reaction are shown in Figure 4. The mass difference of 89 Da ($M_{Au} - M_{Ag}$)
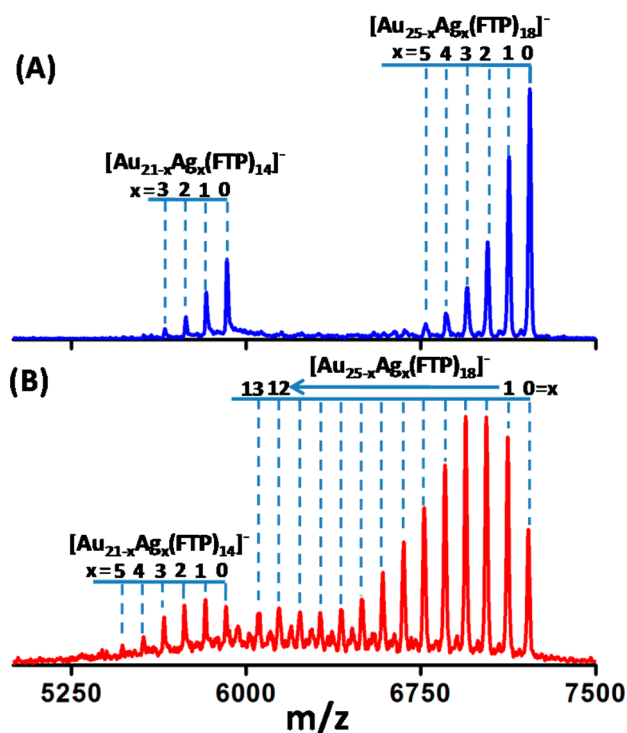
Figure 4. Negative ion mode MALDI MS spectra showing the time-dependent changes in the reaction mixture of $Au_{25}(FTP)_{18}$ and $Ag_{44}(FTP)_{30}$ after 1 h (A) and 3 h (B) of the reaction. $[Au_{21-x}Ag_x(FTP)_{14}]^-$ are the fragments from the alloy clusters due to the loss of $Au_4(FTP)_4$ (see Figure S1).

between the peaks in group I clearly confirms the formation of $Au_{25-x}Ag_x(FTP)_{18}$ clusters. This shows that Ag inclusion of 1–5 atoms and 1–13 atoms was observed after 1 h and 3 h of the reaction, respectively. After 24 h of reaction, Ag inclusion of up to 17 atoms was observed (see Figure S20 and S21). Analysis of the time-dependent MALDI MS data for clusters with same and different ligands (Figures S3–S5 and S20) show that the ligand shell on the clusters plays an important role in controlling their reactivity (see the text associated with Figure S20).

As we observed both metal and ligand incorporations in $Au_{25}(PET)_{18}$, we proceeded to develop an understanding of the sequence of events leading to the formation of $Au_{25-x}Ag_x(PET)_{18-y}(FTP)_y$ clusters. We wanted to see which of the events, FTP-PET, Ag–Au or (Ag-FTP)-(Au-PET) exchange, is the first step. For this, mass spectra of reaction mixtures were measured immediately after mixing the clusters. These measurements shown in Figure 5 reveal that the Ag–Au, (Ag-FTP)-(Au-PET) and FTP-PET exchanges occur even at the beginning of the reaction. Parent $Au_{25}(PET)_{18}$ also undergoes FTP-PET exchange (see the peak (0, 1) in Figure 5A and 5B). However, only one FTP-PET exchange was observed for $Au_{25}(PET)_{18}$ and its relative intensity remained almost the same even at about a 6-fold increase in the concentration of $Ag_{44}(FTP)_{30}$ (see Figure 5A,B). These
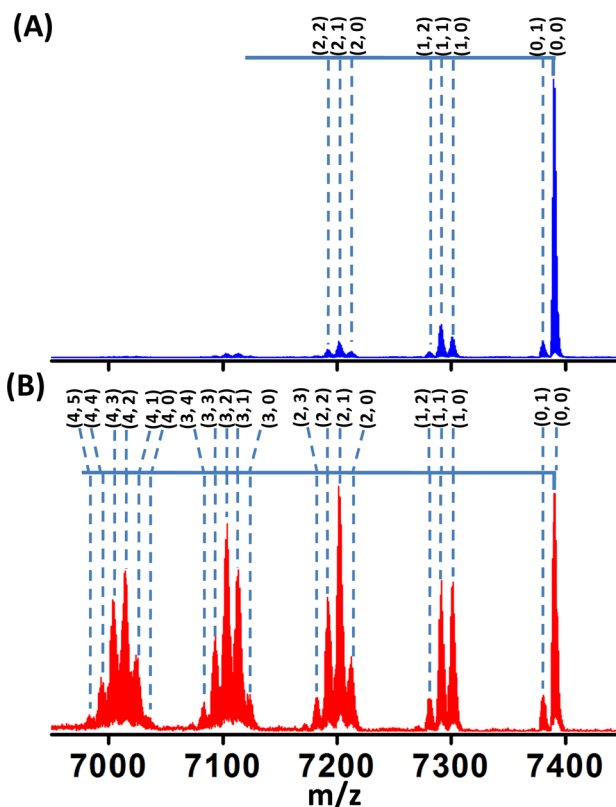
Figure 5. Negative ion mode ESI MS spectra measured immediately after mixing $Au_{25}(PET)_{18}$ with $Ag_{44}(FTP)_{30}$ in the $Au_{25}:Ag_{44}$ ratio 14:1 (A) and 2.5:1.0 (B). The numbers (x, y) in parentheses are according to the general molecular formula, $Au_{25-x}Ag_x(PET)_{18-y}(FTP)_y$.

observations show that Ag–Au and (Ag-FTP)-(Au-PET) exchanges are much faster than pure FTP-PET exchange.

Occurrence of peaks with a separation of m/z 10, in the insets of Figure 3 and Figure S10, may be tempting to conclude that all of these clusters are formed through FTP-PET exchange. For example, the peaks (1, 1) to (1, 4) in Figure S10 may, at first, be considered as the products of sequential FTP-PET exchange of (1, 0) cluster. Mass spectral measurements immediately after mixing (Figure 5 and S22) the clusters reveal that this is not the case. Comparison of Figure 5A and 5B shows that while the relative intensities of the (1, 0) and (1, 1) peaks significantly increases with concentration of $Ag_{44}(FTP)_{30}$, there is no such notable increase in the intensity of the (0, 1) peak. Also, as mentioned before, only one peak due to FTP-PET exchange of $Au_{25}(PET)_{18}$ was observed even when the concentration of $Ag_{44}(FTP)_{30}$ was increased about six times, i.e., no (0, 2) or (0, 3) peaks were observed even at higher concentration of $Ag_{44}(FTP)_{30}$. These observations suggest that the clusters (1, 0) and (1, 1) are produced from (0, 0), i.e., the parent $Au_{25}(PET)_{18}$, through Ag–Au and (Ag-FTP)-(Au-PET) exchanges, respectively. For the same reasons, it is unlikely that the (1, 1) clusters are formed by a Ag–Au exchange of (0, 1) because the intensity of the latter is significantly less than that of (0, 0). Even though clusters such as (1, 2) and (2, 3) are observed in the initial stages of reaction (Figure 5A,B), no (0, 2) and (0, 3) clusters were observed. Hence, the (1, 2) and (2, 3) clusters are more likely to be formed by FTP-PET exchange of (1, 1) and (2, 2) clusters and cannot be the result of Ag–Au exchange from (0, 2) and (0, 3) clusters. Thus, it can be concluded that the presence of FTP in the

Table 1. Energies for the Substitution Reaction of (A) Au in $Ag_{44}(SR)_{30}$, (B) Ag in $Au_{25}(SR)_{18}$ and (C) the Overall Reaction Energies (in eV) as a Function of Their Positions in the Product Clusters, $Au_xAg_{44-x}(SR)_{30}$ and $Au_{25-x}Ag_x(SR)_{18}$ for $x = 1$[a]

(A) Location of Au in $Au_xAg_{44-x}(SR)_{30}$	ΔE/eV
Icosahedron (I)	-0.72
Dodecahedron: cube vertex (D_{cv})	-0.14
Dodecahedron: cube face (D_{cf})	-0.32
Staples (S)	-0.48

(B) Location of Ag in $Au_{25-x}Ag_x(SR)_{18}$	ΔE/eV
Central atom (C)	+0.71
Icosahedron (I)	+0.23
Staples (S)	+0.44

(C)

Location of Ag in $Au_{25-x}Ag_x(SR)_{18}$	Locations of Au in $Au_xAg_{44-x}(SR)_{30}$			
	I	D_{cv}	D_{cf}	S
C	-0.015	+0.564	+0.388	+0.226
I	-0.486	+0.093	-0.083	-0.245
S	-0.276	+0.303	+0.127	-0.035

[a]Locations of substitution for each cluster are described in the Computational Details.

$Au_{25-x}Ag_x(PET)_{18-y}(FTP)_y$ clusters formed is mostly due to (Ag-FTP)-(Au-PET) exchanges rather than due to FTP-PET exchanges.

These observations together suggest that $Au_{25-x}Ag_x(PET)_{18-y}(FTP)_y$ clusters were formed principally by two processes: (Ag-FTP)−(Au-PET) and Ag−Au exchanges. For example, the (1, 1) cluster (see Figure 3 for numbering) is formed by the (Ag-FTP)-(Au-PET) exchange from a (0, 0) cluster. The (1, 1) cluster may then undergo Ag−Au or (Ag-FTP)-(Au-PET) exchange, producing (2, 1) or (2, 2) clusters, respectively. These processes continue to give higher Ag- and FTP-incorporated clusters. There may be other complicated events as well.

Transformation of $Au_{25}(SR)_{18}$ into $Au_{25-x}Ag_x(SR)_{18}$ is confirmed from the above measurements. Similarly, our measurements indicate that $Ag_{44}(SR)_{30}$ has been transformed into $Au_xAg_{44-x}(SR)_{30}$ due to its reaction with $Au_{25}(SR)_{18}$. As mentioned earlier, the mass spectral features due to $Ag_{44}(FTP)_{30}$ disappeared immediately after mixing it with $Au_{25}(PET)_{18}$. MALDI MS measurements show the emergence of a broad peak (group II) at m/z higher than that of $Ag_{44}(FTP)_{30}$ (see Figures 2 and S15). Also, the intensity of this peak increased as the concentration of $Ag_{44}(FTP)_{30}$ increased. The difference between the molecular mass of $Ag_{44}(FTP)_{30}$ (m/z 8567) and the maxima of group II peaks, at different time intervals (1−24 h) of the reaction between $Ag_{44}(FTP)_{30}$ and $Au_{25}(FTP)_{18}$, (see Figure S23) suggests the formation of $Au_xAg_{44-x}(FTP)_{30}$ with $x = 14-16$. However, such an analysis may not give accurate compositions of a mixture due to the high energy provided by the MALDI laser. ESI MS measurements (see Figure S24) clearly indicated the formation of a series of clusters with x varying from 0 to 12. MALDI MS could not resolve the features of these individual clusters due to the broadness of the peaks. Recent reports on the $Au_xAg_{44-x}(SR)_{30}$ clusters[15] (prepared from ionic precursors) indicate that the total number of metal atoms is the same and the structural framework of these clusters is similar to that of $Ag_{44}(SR)_{30}$. UV/vis spectra of reaction mixtures at higher concentrations of

$Ag_{44}(FTP)_{30}$ (see Figure S25B) resemble that of previously reported $Au_{12}Ag_{32}(SR)_{30}$ clusters.[15] At lower Ag_{44} concentrations, (Figure S25A) the absorption spectra resemble $Au_{25-x}Ag_x(SR)_{18}$, as seen in previous reports.[16] Hence, our MALDI and ESI MS measurements confirm the formation of $Au_xAg_{44-x}(SR)_{30}$ in the reaction between $Ag_{44}(FTP)_{30}$ and $Au_{25}(SR)_{18}$. Reactions were also carried out with Au_{25} and Ag_{44} clusters of different protecting ligands (n-butanethiol and 4-mercaptobenzoic acid) (see Figures S26 and S27). Our experiments show that similar reactions occur between other types of Ag and Au clusters and even with plasmonic nanoparticles. Experiments are in progress in these directions. A discussion of the possible locations of Ag atoms in the alloy clusters, based on the charge states of $Au_{25}(SR)_{18}$, previous reports of $Au_{25-x}Ag_x(SR)_{18}$ clusters and the recent report of $Au_{25}Ag_2(SR)_{18}$,[16] is given in the Supporting Information. However, analysis of the structures formed requires more work.

(C). DFT Study of Structural Isomers and Reaction Energetics. To understand the driving force behind the reaction, we used DFT to calculate energies of the reactants [$Au_{25}(SR)_{18}$ and $Ag_{44}(SR)_{30}$], the products [$Au_{25-x}Ag_x(SR)_{18}$ and $Au_xAg_{44-x}(SR)_{30}$] and the likely species being exchanged in the intermediate steps such as metal atoms (M), and thiolate fragments (M-SR) (see Tables S1−S7, see Figure S28 for a description of the fragments). We calculated the energy of the overall reaction (i.e., $Au_{25}(SR)_{30} + Ag_{44}(SR)_{30} \rightarrow Au_{25-x}Ag_x(SR)_{18} + Au_xAg_{44-x}(SR)_{30}$) and reaction energies for substitution of metal atom (M = Ag/Au) and metal−thiolate fragments (M-SR) in different combinations of substituent positions in $Au_{25}(SR)_{18}$ and $Ag_{44}(SR)_{30}$, respectively (see Table 1 and Tables S4−S7). The overall reaction, either through M or M-SR substitutions, was found to be exothermic for certain combinations of substituent positions as shown in Table 1C. This can be attributed to the lowering of the total energy by inclusion of (i) Au atoms or Au-SR into $Ag_{44}(SR)_{30}$ and (ii) Ag-SR into $Au_{25}(SR)_{18}$, rather than the inclusion of Ag atoms into $Au_{25}(SR)_{18}$ (see Tables S4−S7). The more exothermic Au atom or Au-SR substitution into

$Ag_{44}(SR)_{30}$ and Ag-SR substitution into $Au_{25}(SR)_{18}$ compensates for the endothermic[17] silver atom inclusion into the $Au_{25}(SR)_{18}$, in contrast to the exothermic Pd or Pt inclusion.[18,19] The details are discussed below.

We investigated which substituent atom (M) or M-SR fragment positions in each cluster were most preferred energetically and the dependence of the reaction energy as a function of the final substituent positions. Initially we calculated the energies of different isomers of $Au_{25-x}Ag_x(SR)_{18}$ and $Au_xAg_{44-x}(SR)_{30}$ for $x = 1$, relative to the unalloyed clusters. For simplicity, we considered events involving one metal atom substitution into $Au_{25}(SR)_{18}$ and $Ag_{44}(SR)_{30}$. There are a large number of symmetry nonequivalent isomers for each substitution; for eg., when $x = 2$ there are 28 isomers for $Au_{25-x}Ag_x(SR)_{18}$.[20] The preferred locations of substituent metal atoms or fragments in the alloy clusters are indicated by the substitution energy differences between the parent clusters and their alloy isomers, listed in Table 1 A and B.

In case of $Au_{25-x}Ag_x(SR)_{18}$, Ag atoms prefer to stay on the icosahedral vertex positions (see Table S2) as in earlier reports.[14a,c] For $Au_xAg_{44-x}(SR)_{30}$, we found that the order of preference of the position of Au atom is the innermost icosahedron (-0.72 eV), followed by the outermost staple atoms (-0.48 eV), and last, the middle dodecahedral positions D_{cv} and D_{cf} (-0.14 and -0.32 eV) (see Table S1). Reaction energies as a function of substituent positions for $Au_{25-x}(SR)_{18}$ and $Au_xAg_{44-x}(SR)_{30}$ in the alloy clusters (Table 1C) suggest that at fewer numbers of substituent metal atoms ($x \leq 12$), the most energetically favored final metal atom positions are in the icosahedral sites in both $Au_{25}(SR)_{18}$ and $Ag_{44}(SR)_{30}$ (-0.486 eV), and next, in the staples of one cluster and the icosahedral core of the other cluster (-0.245 and -0.276 eV). Two further final metal atom positions in both clusters which are slightly less favorable but still exothermic are the D_{cf} position of $Ag_{44}(SR)_{30}$ and the icosahedral core of $Au_{25}(SR)_{18}$ (-0.083 eV) and the staples in both clusters (-0.035 eV), as listed in Table 1C. As mentioned earlier, the similarity of the absorption spectra of the reaction mixture at higher concentrations of $Ag_{44}(SR)_{30}$ (see Figure S25B) with the previously reported $Au_{12}Ag_{32}(SR)_{30}$ also supports this conclusion that Au atoms preferably occupy the icosahedral core of $Au_xAg_{44-x}(SR)_{30}$, and that for $x = 12$, the $Au_{12}Ag_{32}(SR)_{30}$ structure would be identical to that of the reported crystal structure of $Au_{12}Ag_{32}(SR)_{30}$.[2e]

We considered the energetics of Au-SH and Ag-SH fragments in the unalloyed clusters, and compared this with the energetics of single metal atom substitution to obtain further clues on the mechanism and its driving force. There are three possible Au-SR fragment positions in $Au_{25}(SR)_{18}$ and four different Ag-SR fragments in $Ag_{44}(SR)_{30}$, as shown in Figure S28.

Reaction energies suggest that Ag-SR substitution in $Au_{25}(SR)_{18}$ is more favorable than the Ag atom exchange in the corresponding position, as seen by comparing the substitution energies in Tables S6 and S7. We also note that the endothermic Ag atom substitution in the icosahedral core of $Au_{25}(SR)_{18}$ ($+0.22$ eV) becomes slightly exothermic (-0.01 eV) in the case of the Ag-SR fragment (fragment F3 in Figure S28A) involving an icosahedral Ag atom. In contrast, the Au-SR fragment exchanges in $Ag_{44}(SR)_{30}$ are slightly less favorable than Au atom substitution, but nevertheless still exothermic for the majority of fragment positions (Tables S4 and S5). The substitution energies for the different combinations of final fragment positions in $Ag_{44}(SR)_{30}$ indicate that the exchange of

fragments involving the terminal ligand and the staple Ag atoms (F1 and F2) are energetically more favored compared to the exchange of fragments involving bridging ligand and Ag atoms in D_{cf} positions (F3). However, in the case of $Au_{25}(SR)_{18}$, the exchange of fragment F3 involving icosahedral Au atoms is the most favored energetically followed by exchange between the fragments (F1 and F2) containing the staple atoms of both clusters. Overall, the exchange of M-SR fragments between the clusters is an energetically favorable process due to (i) the exothermic Au-SR substitutions in specific positions (F1, F2 and F4) of $Ag_{44}(SR)_{30}$, (ii) less endothermic (for F1 and F2) and exorthermic (for F3) Ag-SR fragment substitutions in $Au_{25}(SR)_{18}$ (see Tables S5 and S7).

(D). Mechanistic Aspects of the Reaction. We suggest that the metal−thiolate interface plays a significant role in the mechanism of the reaction. In thiolate-protected molecular metal clusters, these interfaces often assume the form of metal−thiolate staple/mount motifs.[2] Atoms in these motifs are considered to be in M^I oxidation state while those in the core are considered to be in M^0 oxidation state. Ag clusters and nanoparticles reduce Au^I or Au^I−SR thiolates[8b,c] due to the higher reduction potential of Au^I. At the sub-nanometer scale, conversely, gold clusters can also reduce Ag^I ions and Ag^I-thiolates,[9] even though such reduction is not feasible for the bulk forms of these metals. Therefore, redox processes might also occur between the clusters since they are composed of silver and gold atoms in both the M^0 and M^I states. The relative energies of the HOMO (d derived) and LUMO (sp derived) states of the $Au_{25}(SR)_{18}$ and $Ag_{44}(SR)_{30}$ and their alloy isomers determine the feasibility of electron transfer from one cluster to another and which would behave like donor or acceptor. The HOMO level of $Ag_{44}(SR)_{30}$ is about 3.8 eV higher than the LUMO of $Au_{25}(SR)_{18}$ (see Table S8 and S9). This indicates that an electron transfer into the states above the LUMO of $Au_{25}(SR)_{18}$ followed by non-radiative relaxation into other levels of the cluster would release enough energy to overcome activation energy barriers and to break bonds, possibly in the staples and the core, leading to partial fragmentation. Although both the clusters are overall negatively charged, locally the electric field in the neighborhood of the ligands is both inhomogeneous[21] and screened by the solvent molecules. Metallophilic interactions between the Au(I) and Ag(I) centers (closed shell species),[22,23] could also occur if their relative orientations permit closer approach within less than 3−4 Å. Attractive π−π stacking interactions between these aromatic ligands may also occur. These interactions are expected to bring clusters into proximity and to find their suitable orientation.

The observed intercluster reactions might occur via the following three stages. In the first stage, destabilization of clusters can occur upon their closer approach facilitated by redox processes and/or metallophilic/π−π interactions. These factors could weaken the M−S bonds in the staples and may result in fragmentation. However, the exact reason behind the destabilization and fragmentation of the clusters cannot be understood from the present studies.

In the next stage, the unstabilized clusters might undergo fragmentation to form small M-SR, M-$(SR)_2$, $M_2(SR)_3$, etc. units or clusters with partially opened staples or mounts followed by the nucleophilic attack of these fragments onto the staples of the cluster. Considering the polar nature of the M-S bonds in the staples due to greater electronegativity of the sulfur atom, these fragments become nucleophilic in nature. Anionic fragments such as $M(SR)_2$ and $M_2(SR)_3$ (where M =

Au/Ag), etc., have been observed in mass spectrometry of $Au_{25}(SR)_{18}$ and $Ag_{44}(SR)_{30}$.[24,2e,g] Among these fragments, Au-$(SR)_2$ and the $Ag(SR)_2$ are the two most abundant species (see Figure S31) and may be the most probable nucleophiles in the reaction. Similar mechanisms have been observed in ligand exchange reactions of monolayer protected clusters[6k] and metal exchange reactions of small metal–thiolate complexes.[25] However, we note that mechanisms of metal exchange in monolayer protected clusters have not yet been investigated thoroughly.

The proposed mechanism for the reaction between $Au_{25}(SR)_{18}$ and $Ag(SR)_2$ fragment resulting in the exchange of Au atoms and various Au-SR fragments is depicted in Schemes S1 and S2. However, in the case of $Ag_{44}(SR)_{30}$ these reactions could consist of several steps of bond-breaking events due to the more complicated bonding network of the $Ag_2(SR)_5$ mounts. This mechanism shows that even though the M-$(SR)_2$ unit is involved in the reaction, the net result is the inclusion of either M or M-SR groups depending on the specific reaction pathways. The exchange of the Ag-SR and Au-SR units between the clusters could be facile as they may be considered to be isolobal fragments. Exchange of similar metal–ligand isolobal units are also commonly encountered in coordination complexes.[26]

In the final stage of the reaction, the open staples or the mounts of the clusters now containing the substituent can rearrange, reconstructing the overall structural framework with substituted metal atoms or ligands resulting in the final products.

An intuitive and alternative way of visualizing the structural changes during the reactions can be inferred from the recent structural model of aspicules[20] showing that $Au_{25}(SR)_{18}$ can be viewed as three interlocked (Borromean) $Au_8(SR)_6$ rings around the central gold atom (see Figure S29). These rings in the destabilized clusters may undergo opening, and once the staple chains or mounts are opened, they become more flexible and assume elongated conformations which gives the atoms of their free ends greater reach with which to interact with the corresponding open chains or mounts on the other cluster. A similar reorganization of the staples has been proposed (theoretically) earlier.[27] The ends of the open chains or mounts can interact more easily exchanging the M and the M-SR units between them. The ring model of $Au_{25}(SR)_{18}$ also suggests that inclusion of Ag into the Au_{13} core is not as significantly hindered from the steric factors as might be expected when $Au_{25}(SR)_{18}$ is viewed as separate core covered by $Au_2(SR)_3$ staples. The opening and reorganization of the chains or mounts away from the core would make the core atoms more exposed, and facile for reaction. This may also be facilitated by structural rearrangements in the core and staples, or $Au_8(SR)_6$ rings as a whole due to rearrangements in the positions of the individual $Au_8(SR)_6$-rings. Similarly, the icosahedral Ag atoms in $Ag_{44}(SR)_{30}$ become more accessible when certain Ag–S bonds are broken (see Figure S30). Thus, our mechanistic model implies that M and M-SR substitutions in the staples can originate from the reactions and rearrangements involving the metal–thiolate fragments and the open chains and mounts, while substitutions of the core atoms could involve the exposed core of one of the clusters and the fragments or open chains or mounts of the other cluster.

The initially formed alloy clusters with fewer numbers of substituents could also undergo similar reactions producing clusters with higher number of substituents until the

thermodynamic equilibrium for the particular reactant concentration is reached (see Figure S4–S5). Final positions of the substituent metal atoms in the alloy clusters are dictated by their relative energies which depend on the number and positions of substituents, as mentioned earlier.

◼ CONCLUSIONS

In conclusion, we report the first example of intercluster reactions of monolayer protected noble metal clusters. Metal core-thiolate interfaces of these clusters play an important role in these reactions. The reaction results in exchange of the metal atoms as well as the metal–thiolate fragments. The intercluster reaction route seems to be a more facile way than the coreduction route and thiolate reaction route[10a] for bimetallic clusters. DFT calculations show that in case of $Au_xAg_{44-x}(SR)_{30}$, Au atoms prefer to occupy the icosahedral core followed by the outer staples and last the inner dodecahedron. Calculations also revealed that the overall reaction is energetically favorable due to the lowering of the energy of Au or Au-SR substitution into $Ag_{44}(SR)_{30}$ rather than the Ag or Ag-SR substitution into $Au_{25}(SR)_{18}$. A discussion of some of the essential aspects of the reaction mechanism is presented. Further experimental and theoretical efforts are needed to understand the phenomena behind these reactions in detail. We hope that our work will draw greater attention to the role of the monolayers in determining the chemistry of these clusters and the role of metallic core and the surrounding monolayers in determining the chemistry of these clusters.

◼ ASSOCIATED CONTENT

ⓢ Supporting Information

The Supporting Information is available free of charge on the ACS Publications website at DOI: 10.1021/jacs.5b09401.

> Instrumentation, general methods of ESI MS and MALDI MS measurements, computational details, temporal changes in absorption and emission spectra during intercluster reactions, additional ESI MS and MALDI MS spectra, discussion on the charge state of the alloy clusters formed and the position of the Ag atoms in them. (PDF)

◼ AUTHOR INFORMATION

Corresponding Author

*pradeep@iitm.ac.in

Present Address

†Currently a postdoctoral fellow at Dept. of Chemistry, University of Illinois at Urbana Champaign.

Notes

The authors declare no competing financial interest.

◼ ACKNOWLEDGMENTS

◼ REFERENCES

(1) (a) Kappes, M. M. *Chem. Rev.* **1988**, *88*, 369. (b) Schmid, G. *Chem. Rev.* **1992**, *92*, 1709. (c) Moskovits, M. *Annu. Rev. Phys. Chem.* **1991**, *42*, 465. (d) Luo, Z.; Smith, J. C.; Woodward, W. H.; Castleman, A. W., Jr. *J. Phys. Chem. Lett.* **2012**, *3*, 3818. (e) Luo, Z.; Gamboa, G.

U.; Smith, J. C.; Reber, A. C.; Reveles, J. U.; Khanna, S. N.; Castleman, A. W., Jr. *J. Am. Chem. Soc.* **2012**, *134*, 18973.

(2) (a) Heaven, M. W.; Dass, A.; White, P. S.; Holt, K. M.; Murray, R. W. *J. Am. Chem. Soc.* **2008**, *130*, 3754. (b) Akola, J.; Walter, M.; Whetten, R. L.; Häkkinen, H.; Grönbeck, H. *J. Am. Chem. Soc.* **2008**, *130*, 3756. (c) Zhu, M.; Aikens, C. M.; Hollander, F. J.; Schatz, G. C.; Jin, R. *J. Am. Chem. Soc.* **2008**, *130*, 5883. (d) Jadzinsky, P. D.; Calero, G.; Ackerson, C. J.; Bushnell, D. A.; Kornberg, R. D. *Science* **2007**, *318*, 430. (e) Desireddy, A.; Conn, B. E.; Guo, J.; Yoon, B.; Barnett, R. N.; Monahan, B. M.; Kirschbaum, K.; Griffith, W. P.; Whetten, R. L.; Landman, U.; Bigioni, T. P. *Nature* **2013**, *501*, 399. (f) Bakr, O. M.; Amendola, V.; Aikens, C. M.; Wenseleers, W.; Li, R.; Negro, L. D.; Schatz, G. C.; Stellacci, F. *Angew. Chem.* **2009**, *121*, 6035. (g) Harkness, K. M.; Tang, Y.; Dass, A.; Pan, J.; Kothalawala, N.; Reddy, V. J.; Cliffel, D. E.; Demeler, B.; Stellacci, F.; Bakr, O. M.; McLean, J. A. *Nanoscale* **2012**, *4*, 4269. (h) Abdulhalim, L. G.; Ashraf, S.; Katsiev, K.; Kirmani, A. R.; Kothalawala, N.; Anjum, D. H.; Abbas, S.; Amassian, A.; Stellacci, F.; Dass, A.; Hussain, I.; Bakr, O. M. *J. Mater. Chem. A* **2013**, *1*, 10148. (i) Schnöckel, H.; Schnepf, A.; Whetten, R. L.; Schenk, C.; Henke, P. *Z. Anorg. Allg. Chem.* **2011**, *637*, 15. (j) Schnöckel, H. *Chem. Rev.* **2010**, *110*, 4125. (k) Schnepf, A.; Schnöckel, H. *Angew. Chem., Int. Ed.* **2014**, *53*, 3064. (l) Rao, T. U. B.; Nataraju, B.; Pradeep, T. *J. Am. Chem. Soc.* **2010**, *132*, 16304. (m) Hassinen, J.; Pulkkinen, P.; Kalenius, E.; Pradeep, T.; Tenhu, H.; Häkkinen, H.; Ras, R. H. A. *J. Phys. Chem. Lett.* **2014**, *5*, 585. (n) Azubel, M.; Koivisto, J.; Malola, S.; Bushnell, D.; Hura, G. L.; Koh, A. L.; Tsunoyama, H.; Tsukuda, T.; Pettersson, M.; Häkkinen, H.; Kornberg, R. D. *Science* **2014**, *345*, 909. (o) Xu, W. W.; Gao, Y. *J. Phys. Chem. C* **2015**, *119*, 14224. (p) Gao, Y. *J. Phys. Chem. C* **2013**, *117*, 8983. (q) Joshi, C. P.; Bootharaju, M. S.; Alhilaly, M. J.; Bakr, O. M. *J. Am. Chem. Soc.* **2015**, *137*, 11578. (r) Yan, J.; Su, H.; Yang, H.; Malola, S.; Lin, S.; Häkkinen, H.; Zheng, N. *J. Am. Chem. Soc.* **2015**, *137*, 11880.

(3) (a) Li, G.; Liu, C.; Lei, Y.; Jin, R. *Chem. Commun.* **2012**, *48*, 12005. (b) Yu, C.; Li, G.; Kumar, S.; Kawasaki, H.; Jin, R. *J. Phys. Chem. Lett.* **2013**, *4*, 2847. (c) Oliver-Meseguer, J.; Cabrereo-Antonino, J. R.; Domínguez, I.; Leyva-Pérez, A.; Corma, A. *Science* **2012**, *338*, 1452. (d) Yamazoe, S.; Koyasu, K.; Tsukuda, T. *Acc. Chem. Res.* **2014**, *47*, 816. (e) Maity, P.; Xie, S.; Yamauchi, M.; Tsukuda, T. *Nanoscale* **2012**, *4*, 4027.

(4) (a) Kwak, K.; Kumar, S. S.; Pyo, K.; Lee, D. *ACS Nano* **2014**, *8*, 671. (b) Kumar, S. S.; Kwak, K.; Lee, D. *Anal. Chem.* **2011**, *83*, 3244. (c) Kwak, K.; Kumar, S. S.; Lee, D. *Nanoscale* **2012**, *4*, 4240. (d) Yuan, X.; Luo, Z.; Yu, Y.; Yao, Q.; Xie, J. *Chem. - Asian J.* **2013**, *8*, 858. (e) Xie, J.; Zheng, Y.; Ying, J. Y. *Chem. Commun.* **2010**, *46*, 961. (f) Zheng, K.; Yuan, X.; Goswami, N.; Zhang, Q.; Xie, J. *RSC Adv.* **2014**, *4*, 60581.

(5) (a) Jin, R. *Nanoscale* **2010**, *2*, 343. (b) Udayabhaskararao, T.; Pradeep, T. *J. Phys. Chem. Lett.* **2013**, *4*, 1553. (c) Mathew, A.; Pradeep, T. *Part. Part. Syst. Charact.* **2014**, *31*, 1017.

(6) (a) Song, Y.; Murray, R. W. *J. Am. Chem. Soc.* **2002**, *124*, 7096. (b) Guo, R.; Song, Y.; Wang, G.; Murray, R. W. *J. Am. Chem. Soc.* **2005**, *127*, 2752. (c) Parker, J. F.; Kacprzak, K. A.; Lopez-Acevedo, O.; Häkkinen, H.; Murray, R. W. *J. Phys. Chem. C* **2010**, *114*, 8276. (d) Dass, A.; Holt, K.; Parker, J. F.; Feldberg, S. W.; Murray, R. W. *J. Phys. Chem. C* **2008**, *112*, 20276. (e) Heinecke, C. L.; Ni, T. W.; Malola, S.; Mäkinen, V.; Wong, O. A.; Häkkinen, H.; Ackerson, C. J. *J. Am. Chem. Soc.* **2012**, *134*, 13316. (f) Ni, T. W.; Tofanelli, M. A.; Phillips, B. D.; Ackerson, C. J. *Inorg. Chem.* **2014**, *53*, 6500. (g) Shichibu, Y.; Negishi, Y.; Tsukuda, T.; Teranishi, T. *J. Am. Chem. Soc.* **2005**, *127*, 13464. (h) Shibu, E. S.; Muhammed, M. A. H.; Tsukuda, T.; Pradeep, T. *J. Phys. Chem. C* **2008**, *112*, 12168−12176. (i) Muhammed, M. A. H.; Shaw, A. K.; Pal, S. K.; Pradeep, T. *J. Phys. Chem. C* **2008**, *112*, 14324. (j) AbdulHalim, L. G.; Kothalawala, N.; Sinatra, L.; Dass, A.; Bakr, O. M. *J. Am. Chem. Soc.* **2014**, *136*, 15865. (k) Fernando, A.; Aikens, C. M. *J. Phys. Chem. C* **2015**, *119*, 20179. (l) Pengo, P.; Bazzo, C.; Boccalon, M.; Pasquato, L. *Chem. Commun.* **2015**, *51*, 3204.

(7) Bootharaju, M. S.; Deepesh, G. K.; Udayabhaskararao, T.; Pradeep, T. *J. Mater. Chem. A* **2013**, *1*, 611.

(8) (a) Bootharaju, M. S.; Pradeep, T. *Langmuir* **2011**, *27*, 8134. (b) Krishnadas, K. R.; Udayabhaskararao, T.; Choudhury, S.; Goswami, N.; Pal, S. K.; Pradeep, T. *Eur. J. Inorg. Chem.* **2014**, *5*, 908−916. (c) Udayabhaskararao, T.; Sun, Y.; Goswami, N.; Pal, S. K.; Balasubramanian, K.; Pradeep, T. *Angew. Chem., Int. Ed.* **2012**, *51*, 2155. (d) Chakraborty, I.; Rao, T. U. B.; Pradeep, T. *J. Hazard. Mater.* **2012**, *211−212*, 396.

(9) (a) Choi, J.-P.; Fields-Zinna, C. A.; Stiles, R. L.; Balasubramanian, R.; Douglas, A. D.; Crowe, M. C.; Murray, R. W. *J. Phys. Chem. C* **2010**, *114*, 15890. (b) Wu, Z. *Angew. Chem., Int. Ed.* **2012**, *51*, 2934−2938. (c) Wang, M.; Wu, Z.; Chu, Z.; Yang, J.; Yao, C. *Chem. - Asian J.* **2014**, *9*, 1006.

(10) (a) Wang, S.; Song, Y.; Jin, S.; Liu, X.; Zhang, J.; Pei, Y.; Meng, X.; Chen, M.; Li, P.; Zhu, M. *J. Am. Chem. Soc.* **2015**, *137*, 4018. (b) Zhu, M.; Chan, G.; Qian, H.; Jin, R. *Nanoscale* **2011**, *3*, 1703.

(11) Som, A.; Samal, A. K.; Udayabhaskararo, T.; Bootharaju, M. S.; Pradeep, T. *Chem. Mater.* **2014**, *26*, 3049.

(12) (a) Shichibu, Y.; Negishi, Y.; Watanabe, T.; Chaki, N. K.; Kawaguchi, H.; Tsukuda, T. *J. Phys. Chem. C* **2007**, *111*, 7845. (b) Wang, S.; Meng, X.; Das, A.; Li, T.; Song, Y.; Cao, T.; Zhu, X.; Zhu, M.; Jin, R. *Angew. Chem., Int. Ed.* **2014**, *53*, 2376−2380.

(13) Negishi, Y.; Iwai, T.; Ide, M. *Chem. Commun.* **2010**, *46*, 4713.

(14) (a) Kumara, C.; Aikens, C. M.; Dass, A. *J. Phys. Chem. Lett.* **2014**, *5*, 461. (b) Yamazoe, S.; Kurashige, W.; Nobusada, K.; Negishi, Y.; Tsukuda, T. *J. Phys. Chem. C* **2014**, *118*, 25284. (c) Guidez, E. B.; Mäkinen, V.; Häkkinen, H.; Aikens, C. M. *J. Phys. Chem. C* **2012**, *116*, 20617.

(15) Yang, H.; Wang, Y.; Huang, H.; Gell, L.; Lehtovaara, L.; Malola, S.; Häkkinen, H.; Zheng, N. *Nat. Commun.* **2013**, *4*, 2422.

(16) Yao, C.; Chen, J.; Li, M.-B.; Liu, L.; Yang, J.; Wu, Z. *Nano Lett.* **2015**, *15*, 1281.

(17) Walter, M.; Moseler, M. *J. Phys. Chem. C* **2009**, *113*, 15834.

(18) Negishi, Y.; Kurashige, W.; Niihori, Y.; Iwasab, T.; Nobusada, K. *Phys. Chem. Chem. Phys.* **2010**, *12*, 6219.

(19) Guidez, E. B.; Mäkinen, V.; Häkkinen, H.; Aikens, C. M. *J. Phys. Chem. C* **2012**, *116*, 20617.

(20) Natarajan, G.; Mathew, A.; Negishi, Y.; Whetten, R. L.; Pradeep, T. *J. Phys. Chem. C* **2015**, *119*, 27768.

(21) Chen, X.; Moore, J. E.; Zekarias, M.; Jensen, L. *Nat. Commun.* **2015**, *6*, 8921.

(22) Ni, W.-X.; Qiu, Y.-M.; Li, M.; Zheng, J.; Sun, R. W.-Y.; Zhan, S.-Z.; Ng, S. W.; Li, D. *J. Am. Chem. Soc.* **2014**, *136*, 9532.

(23) Nardi, M. D.; Antonello, S.; Jiang, D.; Pan, F.; Rissanen, K.; Ruzzi, M.; Venzo, A.; Zoleo, A.; Maran, F. *ACS Nano* **2014**, *8*, 8505.

(24) Angel, L. A.; Majors, L. T.; Dharmaratne, A. C.; Dass, A. *ACS Nano* **2010**, *4*, 4691.

(25) (a) Autissier, V.; Henderson, R. A. *Inorg. Chem.* **2008**, *47*, 6393. (b) Hagen, K. S.; Stephan, D. W.; Holm, R. H. *Inorg. Chem.* **1982**, *21*, 3928.

(26) (a) Goldman, A. S.; Tyler, D. R. *J. Am. Chem. Soc.* **1986**, *108*, 89. (b) Hor, T. S. A.; Tan, A. L. C. *J. Coord. Chem.* **1989**, *20*, 311.

(27) Liu, C.; Lin, S.; Pei, Y.; Zeng, X. C. *J. Am. Chem. Soc.* **2013**, *135*, 18067.

(28) Enkovaara, J.; et al. *J. Phys.: Condens. Matter* **2010**, *22*, 253202.